APPLIED PHYSICS

Acoustic topological beam nonreciprocity via the rotational Doppler effect

Quansen Wang[1]†, Zhiling Zhou[2]†, Dongmei Liu[1]†, Hua Ding[2], Min Gu[1]*, Yong Li[2]*

Reciprocity is a fundamental principle of wave physics related to time-reversal symmetry. Nonreciprocal wave behaviors have been pursued for decades because of their great scientific significance and tremendous potential applications. However, nonreciprocity devices have been based on manipulation of non-topological charge (TC) in most studies to date. Here, we introduce the rotational Doppler effect (RDE) into the acoustic system to achieve nonreciprocal control of the TC beam. We use the metasurface to generate a vortex beam with a defined TC. By rotating the metasurface with specific angular velocity, the wave vector of the transmitted wave obtains positive and negative transition flexibly due to the RDE. As a result, isolated and propagating states of the vortex beam can be realized by controlling the rotation direction, representing nonreciprocal propagation. Our work also provides an alternative method for the application of TC beams and the realization of nonreciprocity.

INTRODUCTION

Reciprocity is one of the most fundamental principles in wave physics and is applied in electromagnetics (*1*), optics (*2*), and acoustics (*3*). Note that reciprocal propagation describes when the excitation source is exchanged with the observation point location. The response of the transmitted port is symmetric. It also means that the special transmission characteristic is closely related to the time-reversal symmetry (*4*). Breaking this bidirectional transmission characteristic, realizing unidirectional transmission plays a vital role in many applications and has become a hotspot of current research. For example, in the optical and thermal fields (*5*–*9*), unidirectionality is mainly achieved by using additional phase changes (*10*, *11*) or special nonlinear effects (*12*–*17*). These approaches also offer an entirely new way of thinking about the implementation of optical computers and thermal energy control. In particular, the acoustic nonreciprocal isolators is realized mainly by nonlinear mechanisms through various effects (*12*–*16*). For example, an acoustic diode is formed by coupling a superlattice with a strongly nonlinear medium or a layer of ultrasound contrast agent microbubble suspension (*12*, *13*), and the Zeeman effect is formed by introducing external excitation to split the resonance mode, resulting in a change in the wave vector state (*16*). These proposed nonreciprocal devices have also brought new ideas in detection, imaging, and information exchange (*13*, *18*–*20*).

In optics, Allen proposed a spin-independent polarization beam in 1992, which has a spiral phase distribution of $\exp(im\theta)$ (*21*). Each photon has "*mh*" orbital angular momentum (OAM), where m is the OAM quantum number, i.e., the topological charge (TC). This light beam with OAM is also called a vortex beam (VB). When the observer and the VB rotate in the same or opposite direction, it is found that the actually observed VB has a frequency shift compared with the under static conditions, which shares a similar physical principle with the linear Doppler effect due to the linear motion of the source or observer. The difference is that the linear Doppler effect is caused by the linear motion in the Cartesian coordinate system, while the deviation under the dynamic VB is caused by the linear motion in the polar coordinate system. Consequently, this is called the rotational Doppler effect (RDE) (*22*). The existence of the RDE has also been verified in optics (*23*–*26*) and radio (*27*, *28*). Meanwhile, the cloaking of the object and the determination of the rotating object's rotation speed have been demonstrated by using this unique property (*29*–*32*). Note that the TC beam exists not only in transverse waves but also in longitudinal waves (*33*–*35*), which means that the RDE also exists in sound waves. Gibson and colleagues used the equivalent relationship of the acoustic-optic Doppler effect to determine the measurement method of the rotation speed of the black hole (*36*, *37*), which provided a new idea for the application of the RDE. In recent works, the isolation of plane electromagnetic wave (TC = 0) has been well realized by combing space-time encoding metasurface with RDE (*38*).

Inspired by the RDE in optics, we achieve nonreciprocal acoustic isolation based on topological beam evolution by introducing RDE to a passive metasurface. By using active control, the rotation of the metasurface can be a new implementation of nonreciprocal isolation. This way and research object are essentially distinct from the previous studies. We extend the nonreciprocal research object from the plane wave (TC = 0) to the sound beam with TC by exploiting the rotational degrees of freedom of RDE. The isolated and propagating states are respectively controlled with positive and negative rotational direction and speed. Benefiting from the mechanical rotation, we break the constraints of using nonlinear acoustic media and nonlinear acoustic effects to achieve nonreciprocal acoustic isolation. The fast and flexible evolution of the topological beam between the propagation and isolation is realized. More essentially, our research shows that the introduction of RDE can provide an alternative solution for the manipulation and application of topological beams.

RESULTS

Principle of the acoustic RDE and nonreciprocal transmission

The prerequisite for generating the RDE is the generation of VB with a defined TC. Several ways to generate VB have also been reported in acoustics, such as spiral gradient plates (*34*), ultrasonic

[1]Guangdong Provincial Key Laboratory of Quantum Engineering and Quantum Materials, South China Normal University, Guangzhou, China. [2]Institute of Acoustics, School of Physics Science and Engineering, Tongji University, Shanghai, China.
*Corresponding author. Email: mingu@m.scnu.edu.cn (M.G.); yongli@tongji.edu.cn (Y.L.)
†These authors contributed equally to this work.

arrays (*39*), and Helmholtz cavities (*35*). We take the cascaded double-opening Helmholtz cavity as an example to generate a VB with a defined TC to meet the prerequisites for achieving the RDE. When a plane wave passes through a static metasurface, a VB with a certain TC can be generated at the transmission port because of the influence of the passive structure on the wave vector control (Fig. 1A). With the initiation of structural rotation, the RDE is introduced into the system. Affected by the rotational speed and direction, the system behaves differently compared with the static situation, enabling sound isolation and "deepening" of the vortex (Fig. 1, B and C).

To describe the influence of metasurface and dynamic degrees of freedom on wave vector regulation and the evolution of the system, we introduce a coordinate with $k_{m,\,n}$, Re(k_z), and Im(k_z) as three perpendicular axes. The system behaves within three states: the vortex state in the static structure (Fig. 1, A and D), the vortex isolation state in the dynamic condition (Fig. 1, B and E), and the vortex propagation state in the dynamic condition (Fig. 1, C and F). The following describe the evolution process of each state. When a plane wave passes through a static passive helical metasurface, the plane wave is evolved into a VB with a certain TC (Fig. 1D). At this time, the axial wave number k_{z1}evolves from k_0 (where $k_0 = 2\pi/\lambda$ is the wave number and λ is the excitation wavelength) into the propagation plane and satisfies $k_{z1} = \sqrt{k_0^2 - k_{1,1}^2}$ (indicated by the gray arrow in Fig.1D) (*35*). To provide additional dynamic degrees of freedom and RDE for the system and the transmission VB, we rotate the structure by motor (Fig. 1, B and C). We can equate it to a statically emitted vortex sound beam into a substructure with a certain spiral gradient (fig. S1). The effect on the transmitted vortex frequency can be expressed as

$$\omega_R = \omega_0 \pm m\Omega \tag{1}$$

where m is the TC, $\omega_0 = 2\pi f$ is the angular frequency of the incident plane wave, f is the excitation frequency of the incident wave, ω_R is the angular frequency of the transmitted wave, $\Omega = 2\pi f_n$ is the angular velocity of the mechanical rotation, and f_n is the rotational speed of the structure. We find that with the addition of the RDE, the system exhibits a secondary change in the propagating wave number k_z, which leads to a change in the acoustic energy flux at the transmission port. The wave number and acoustic energy flux at the transmission port can be expressed as (more details in notes S1)

$$(k_0 \pm k_R)^2 = k_z^2 + k_{m,n}^2 \tag{2}$$

$$\Phi_z = \frac{1}{2\rho_0\omega}\sqrt{1-\frac{k_{m,n}^2}{k_{\text{eff}}^2}}\left|A_{m,n}\right|^2 \tag{3}$$

where k_0 is the wave number of the incident wave, $k_R = 2\pi f_n m/\lambda f$ is the rotation wave number concerning the speed of the object, $k_{m,\,n}$ is the nth positive root of the equation $\frac{\partial J_m(k_{m,n}R)}{\partial k_{m,n}R}\Big|_{R=a} = 0$, which is the radial wave number of the waveguide, k_z is the axial wave number, and $k_{\text{eff}} = k_0 \pm k_R$ is the effective wave number. Equation 3 indicates that when the direction of mechanical rotation is the same as the rotational direction, the excitation wave number k_0 will decrease because of the introduction of the rotational wave number k_R, $k_{\text{eff}} = k_0 - k_R$. When $k_R > k_0 - k_{1,1}$ is satisfied, the axial wave number k_z evolves from propagation plane to isolation plane (indicated by the blue arrow in Fig. 1E). The wave number k_z is transformed from a real number to a purely imaginary number. There is no energy transmission at this time, and the acoustic isolation phenomenon is formed. When the direction of mechanical rotation is opposite to the vortex, the excitation wave number k_0 will increase, $k_{\text{eff}} = k_0 - (-k_R)$.

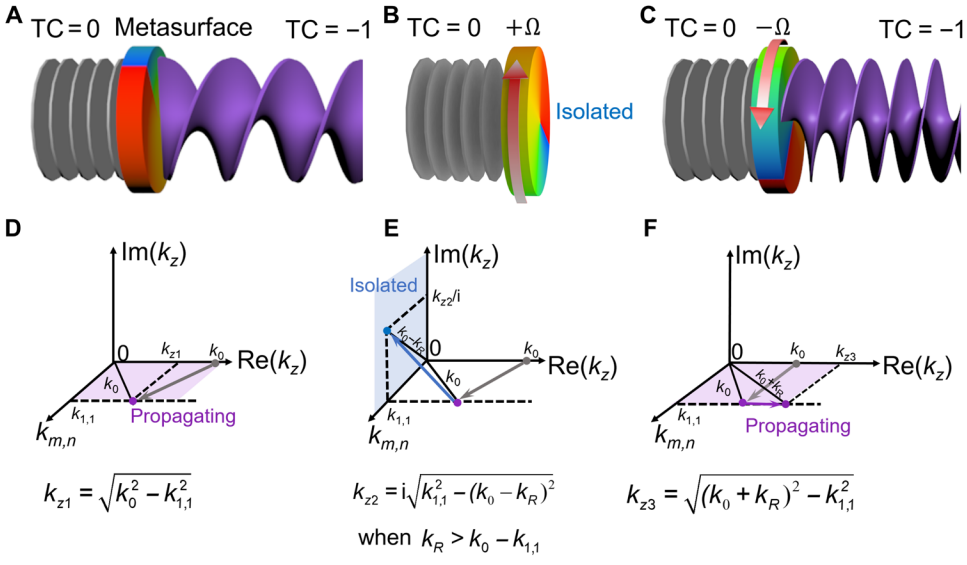

Fig. 1. Principle of nonreciprocal evolution. (**A**) Schematic diagram of the static condition without the RDE. (**B**) When the metasurface and the vortex rotate in the same direction, the incident source is turned off without energy transmission. (**C**) When the metasurface and the vortex rotate in the opposite direction, the incident source usually propagates. (**D**) When the plane wave passes through the passive helical metasurface, the propagating wave number k_z evolves from k_0 to the propagating plane (as indicated by the gray arrow). The propagating wave number satisfies $k_{z1} = \sqrt{k_0^2 - k_{1,1}^2}$, where $k_{1,1}$ is the radial wave number of TC = −1. (**E**) When a plane wave passes through a metasurface that rotates in the same direction as the vortex, the rotation wave number satisfies $k_R > k_0 - k_{1,1}$. The propagation wave number k_z evolves from the propagation plane to the isolation plane. The isolation phenomenon produces no energy transmission at this time. (**F**) When a plane wave passes through a metasurface that rotates in opposition to the vortex, the propagating wave number evolves only in the propagation plane. At this time, the sound wave can propagate normally.

The VB can still propagate normally, and the phenomenon of vortex deepening appears (Fig. 1C). The propagating wave number k_z evolves in the propagation plane and exists as a real number (indicated by the purple arrow in Fig. 1F) (more details in note S1).

Generation of the VB

To prove the accuracy of the above theory, we verify it by using numerical simulations and experiments. Since the realization of the RDE presupposes the generation of an acoustic vortex wave with a defined TC, we take the example of TC = −1, whose structure has a three-dimensionally (3D) printed resin material made and operates at a frequency of 2016 Hz (see Fig. 2A). The radial direction consists of p rows, and each row of planes consists of q sectors. By changing the width w of the straight pipe (Fig. 2B), the phase difference of the two adjacent sectors can satisfy $\varphi = 2\pi \cdot |TC|/q$, to generate a VB with a certain TC at the transmission port. We take two rows of eight sectors as an example to generate an acoustic VB with a TC = −1 to meet the prerequisites for realizing the RDE. The experimental setup and the experimental measurements are reported in note S2 and Methods. Under static conditions, through the numerical simulation of the proposed structure, the phase and acoustic amplitude distributions at the z = λ cross section (see Fig. 2, C and E) demonstrate that our adopted structure can well generate acoustic VB with defined TCs. Moreover, the phase and amplitude distribution measured experimentally at the same position is shown in Fig. 2 (D and F, respectively). Our measurements also corroborate the theoretical predictions of Fig. 2 (C and E), revealing the evolution from TC = 0 to TC = −1 (Fig. 1A). This also provides corresponding guarantees for the implementation of the RDE.

Acoustic RDE

In the previous sections, it is shown that the structure we adopted can well satisfy the preconditions for realizing RDE. To understand the response of the RDE, we show the sound pressure spectrum at different speeds (Fig. 3A), where the isotropic speed is positive and the reverse speed is negative. The measurement method is described in note S2 and Methods. With the start of the metasurface rotation, the system is transformed from static to dynamic. In this case, regardless of whether the metasurface rotates in the same or opposite direction, the transmission signal has an offset on the frequency axis. The offset and the rotational speed satisfy a specific mathematical relationship in which the rotational speed and the transmitted vortex frequency are strictly linear, while the reciprocal of the slope is the same as the TC of the vortex (Fig. 3B). This proves that the same RDE exists in acoustics as in optics. Moreover, our measurements also verify the prediction of Eq. 1.

Nonreciprocal evolution of acoustic topological beam

When the system rotation starts, the RDE is introduced into the system. To gain further insights into the response of the proposed system, we show the sound field distribution for different rotational speeds (see Fig. 4). The transmission acoustic amplitude tends to decrease with increasing corotational speed due to the change in the frequency of the transmitted frequency caused by the structure rotation. When the speed reaches 6 rad/s, the sound field distribution is close to zero, which shows the phenomenon of acoustic isolation (see Figs. 1E and 4, C and F). To avoid the influence of friction noise, we set a specific gap between the sample and the transmission tube, which causes energy loss. Hence, the theoretical value is higher than the experimental value (more details in note S3). Figure 4 shows only the change in sound amplitude and not the change in the acoustic energy flux. To describe the influence of different rotational speeds on system energy under dynamic conditions more clearly (*40*), we characterize this effect by measuring the energy corresponding to each mode at the same position and the total system energy (see Fig. 5). As expected, the transformation of TC = 0

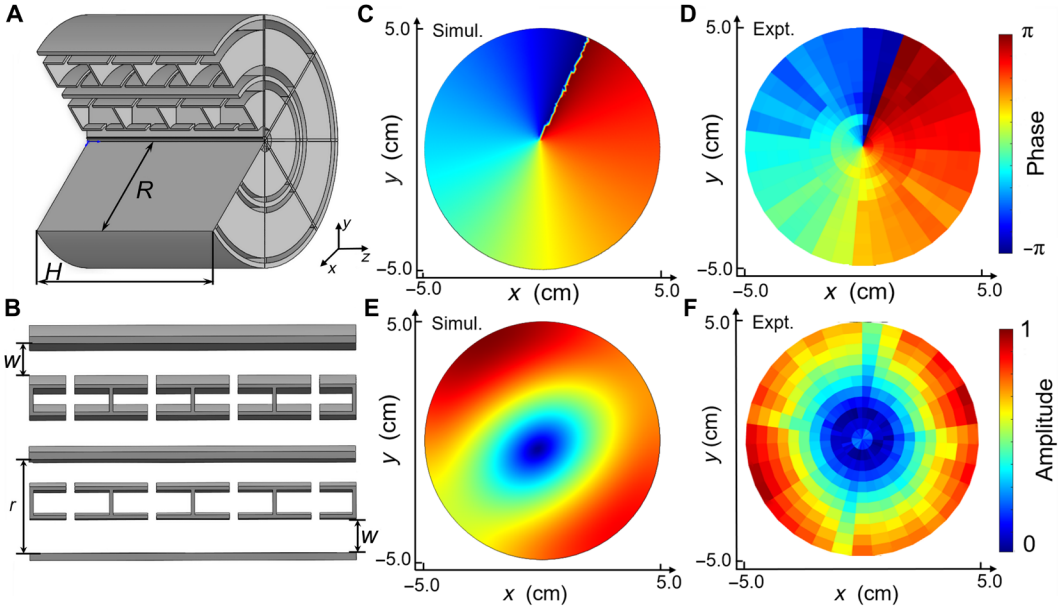

Fig. 2. Vortex generator and VB. (**A**) Schematic diagram of the structure of the vortex generator composed of eight fan-shaped double-opening resonators ($H = 0.5\lambda$ in the z direction; λ is the acoustic wave). (**B**) In the radial direction, a single structure consists of two layers of double-opening resonators (w is the width of the straight tube; radial resolution $R = 2r$). (**C**) Numerically simulated phase distribution at $z = \lambda$. (**D**) Experimentally measured phase distribution at $z = \lambda$. (**E**) Numerically simulated sound field distribution at $z = \lambda$. (**F**) Experimentally measured sound field distribution at $z = \lambda$ ($\lambda = 17$ cm in the air).

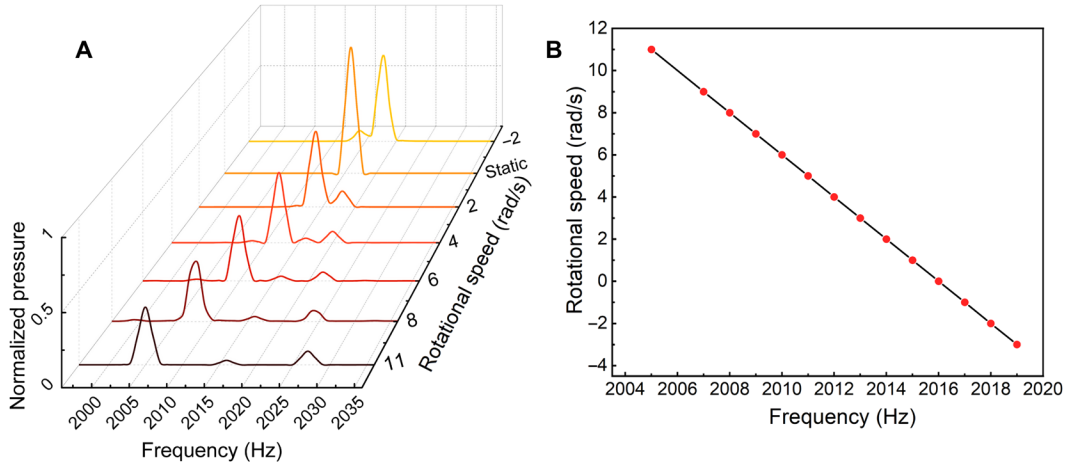

Fig. 3. Experimental observation of the RDE. (**A**) Sound pressure spectrum at different speed conditions. (**B**) Effect of angular velocity on frequency. The measured frequency shift follows a strictly linear relationship with angular velocity, satisfying the theoretical prediction of Eq. 1, and its reciprocal of the slope is the TC of the VB.

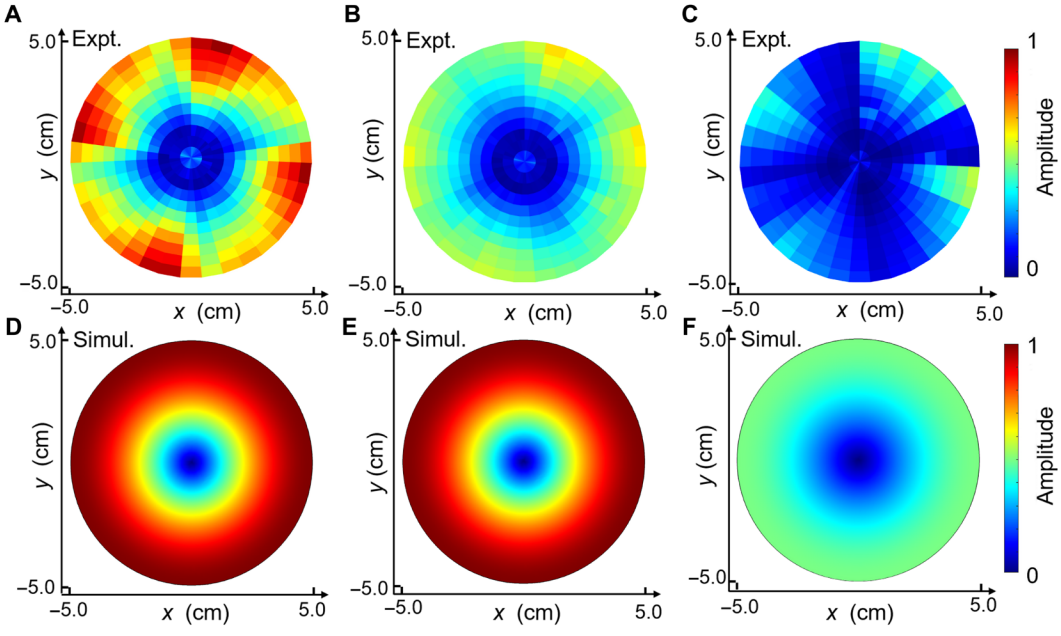

Fig. 4. Evolution of the nonreciprocal state. (**A** to **C**) Experimental sound field distributions at a certain distance from the sample surface ($z = \lambda$) and a speed of 2, 3, and 6 rad/s, respectively. (**D** to **F**) Simulated sound field distributions at a certain distance from the sample surface ($z = \lambda$) and a speed of 2, 3, and 6 rad/s, respectively.

to TC = −1 is achieved with the introduction of the structure (see Figs. 1D and 5A). When the rotational speed Ω is less than 6 rad/s, the total energy of the system decreases with the increase of the rotational speed in the same direction. However, the transmission mode is still the same as the static mode, mainly TC = −1 (Fig. 5A). It also proves that the research object of the RDE is the VB with TC. With the continuous increase in the reverse velocity, the energy of the main mode (TC = −1) in the system continues to increase, and the phenomenon of vortex deepening appears (see Figs. 1F and 5A). When the speed Ω is greater than or equal to 6 rad/s, the energy corresponding to each mode of the system has wholly converged to 0, as has the total energy of the system (see Fig. 5B). That is, the acoustic isolation function is achieved. Our measurements also corroborate the theoretical predictions of Fig. 1E. Therefore, a reciprocal to nonreciprocal evolution is achieved when the rotational speed reaches the target value. However, limited by the actual rotational speed, theoretically, when the isotropic rotational speed increases to infinity, the acoustic isolation function can be realized over a wide range of frequencies. At this moment, the acoustic isolation is affected only by the rotational speed.

To thoroughly verify the unidirectionality of the system, we change the direction of rotation of the structure from isotropic to reverse, which is equivalent to changing the direction of sound wave propagation. At this point, the energy of each mode in the system and the total energy of the system both show an increasing trend. The system can realize normal transmission (see Fig. 5). We have proven that sound insulation and acoustic nonreciprocity can be achieved as long as the rotation direction and rotation speed of

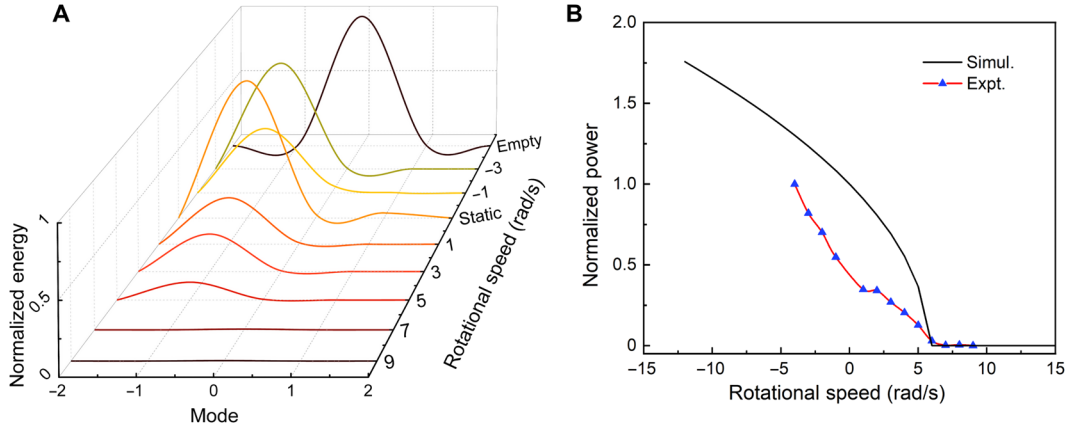

Fig. 5. Experimental characterization of the RDE. (**A**) Energy distribution of each mode at different speeds for different modes, where the energy of each mode tends to decrease as the isotropic speed continues to increase. When the rotational speed Ω is greater than or equal to 6 rad/s, the acoustic isolation phenomenon appears. Here, "Empty" denotes the unstructured static case, and "Static" denotes the static case with structure. (**B**) Trend of the total system energy variation at different rotational speeds. When the isotropic rotational speed Ω is greater than or equal to 6 rad/s, the system shows acoustic isolation. When the rotational speed Ω is less than 6 rad/s, the system can transmit normally.

the structure meet certain conditions. The introduction of this additional physical field also provides a great degree of control and expansion space for control of the system.

DISCUSSION

We have proven through theory and experiment that the same RDE exists in acoustics as in optics. The acoustic isolation and nonreciprocal function of the two ports are realized by this unique phenomenon. This function mainly uses the RDE to provide the system with an additional degree of controllable freedom, which leads to a change in the propagation state. The experimental results verify the numerical simulations and theoretical predictions. This approach also provides a new scheme for achieving acoustic isolation and acoustic nonreciprocity. For different frequencies, the same phenomena can be realized by modulating the rotational speed, which provides a feasible approach for broadband acoustic isolation.

In addition, with the development of related fields such as underwater communication (*41*, *42*) and particle manipulation (*43*), the application potential of topological beams has gradually emerged. At the same time, our findings further expand the freedom of acoustic manipulation and offer the possibility of acoustic logic manipulation and the implementation of underwater acoustic communication.

METHODS

Numerical simulations

The finite element method is used for the numerical study. The resin used to make the samples and the waveguide for transmission were modeled as acoustically rigid materials, where the mass density and sound velocity of the air-filled domain were set to $\rho_0 = 1.21\ kg/m^3$ and $c_0 = 343$ m/s, respectively. To simulate that the proposed metasurface can generate a VB with defined TC (see Fig. 2, C and E) and the change in transmitted sound pressure under dynamic conditions (see Fig. 4, D to F), it can be calculated using the frequency-domain solver. For transmission pressure distributions under dynamic conditions (see Fig. 4, D to F), we simulate the effect of RDE on the transmitted acoustic field by varying the excitation frequency of the ideal VB in the same cylindrical waveguide (more details in note S1).

Experiments

The structure we designed is made of 3D-printed resin material; the two sides of the structure are connected with acrylic tubes with an inner diameter of 100 mm and a wall thickness of 5 mm. A monochromatic sound wave is excited by a loudspeaker at one end and propagates in the waveguide as a plane wave, exciting the intermediate sample. At the end of the waveguide, we filled the wedge-shaped sponge so that the wave only propagates and does not reflect within the domain. Under dynamic conditions, the metasurface is fixed in the bearing, connected by a conveyor belt to the motor to rotate the structure circumferentially (fig. S2). The rotation speed and direction of the structure are adjusted by changing the output amplitude and positive and negative polarity of the DC-regulated power supply. In both static and dynamic experiments, a $^1/_4$-inch-diameter microphone (Brüel & Kjær type 4187) and a multichannel analyzer (Brüel & Kjær type 3160) were used to extract pressure and phase information, and four $^1/_8$-inch-diameter microphones (Brüel & Kjær type 2670) were used to measure energy information. Meanwhile, we stick a highly reflective logo on the side of the sample to obtain accurate rotational speed information. The rotational speed of the structure is measured using laser velocimetry (more details in note S2).

SUPPLEMENTARY MATERIALS

Supplementary material for this article is available at https://science.org/doi/10.1126/sciadv.abq4451

REFERENCES AND NOTES

1. L. D. Landau, J. Bell, M. Kearsley, L. Pitaevskii, E. Lifshitz, J. Sykes, *Electrodynamics of Continuous Media* (Elsevier, 2013), vol. 8.
2. H. Von Helmholtz, *Helmholtz's Treatise on Physiological Optics* (Optical Society of America, 1925), vol. 3.
3. A. D. Pierce, *Acoustics: An Introduction to Its Physical Principles and Applications* (Springer, 2019).
4. D. L. Sounas, A. Alù, Non-reciprocal photonics based on time modulation. *Nat. Photonics* **11**, 774–783 (2017).
5. B. Li, L. Wang, G. Casati, Thermal diode: Rectification of heat flux. *Phys. Rev. Lett.* **93**, 184301 (2004).

6. M. Maldovan, Sound and heat revolutions in phononics. *Nature* **503**, 209–217 (2013).
7. D. Jalas, A. Petrov, M. Eich, W. Freude, S. Fan, Z. Yu, R. Baets, M. Popović, A. Melloni, J. D. Joannopoulos, M. Vanwolleghem, C. R. Doerr, H. Renner, What is—And what is not—An optical isolator. *Nat. Photonics* **7**, 579–582 (2013).
8. D. L. Sounas, C. Caloz, A. Alù, Giant non-reciprocity at the subwavelength scale using angular momentum-biased metamaterials. *Nat. Commun.* **4**, 2407 (2013).
9. D.-W. Wang, H.-T. Zhou, M.-J. Guo, J.-X. Zhang, J. Evers, S.-Y. Zhu, Optical diode made from a moving photonic crystal. *Phys. Rev. Lett.* **110**, 093901 (2013).
10. F. Zangeneh-Nejad, R. Fleury, Doppler-based acoustic gyrator. *Appl. Sci.* **8**, 1083 (2018).
11. M. C. Rechtsman, J. M. Zeuner, Y. Plotnik, Y. Lumer, D. Podolsky, F. Dreisow, S. Nolte, M. Segev, A. Szameit, Photonic Floquet topological insulators. *Nature* **496**, 196–200 (2013).
12. B. Liang, B. Yuan, J.-c. Cheng, Acoustic diode: Rectification of acoustic energy flux in one-dimensional systems. *Phys. Rev. Lett.* **103**, 104301 (2009).
13. B. Liang, X. S. Guo, J. Tu, D. Zhang, J. C. Cheng, An acoustic rectifier. *Nat. Mater.* **9**, 989–992 (2010).
14. T. Devaux, A. Cebrecos, O. Richoux, V. Pagneux, V. Tournat, Acoustic radiation pressure for nonreciprocal transmission and switch effects. *Nat. Commun.* **10**, 3292 (2019).
15. N. Boechler, G. Theocharis, C. Daraio, Bifurcation-based acoustic switching and rectification. *Nat. Mater.* **10**, 665–668 (2011).
16. R. Fleury, L. Sounas Dimitrios, F. Sieck Caleb, R. Haberman Michael, A. Alù, Sound isolation and giant linear nonreciprocity in a compact acoustic circulator. *Science* **343**, 516–519 (2014).
17. L. Wang, B. Li, Thermal logic gates: Computation with phonons. *Phys. Rev. Lett.* **99**, 177208 (2007).
18. T. Devaux, V. Tournat, O. Richoux, V. Pagneux, Asymmetric acoustic propagation of wave packets via the self-demodulation effect. *Phys. Rev. Lett.* **115**, 234301 (2015).
19. Z. Chen, Y. Peng, H. Li, J. Liu, Y. Ding, B. Liang, X.-F. Zhu, Y. Lu, J. Cheng, A. Alù, Efficient nonreciprocal mode transitions in spatiotemporally modulated acoustic metamaterials. *Sci. Adv.* **7**, eabj1198 (2021).
20. Z. Wu, Y. Zheng, K. W. Wang, Metastable modular metastructures for on-demand reconfiguration of band structures and nonreciprocal wave propagation. *Phys. Rev. E* **97**, 022209 (2018).
21. N. B. Simpson, L. Allen, M. J. Padgett, Optical tweezers and optical spanners with Laguerre–Gaussian modes. *J. Modern Opt.* **43**, 2485–2491 (1996).
22. L. Marrucci, Physics. Spinning the Doppler effect. *Science* **341**, 464–465 (2013).
23. Z. Guo, H. Liu, H. Zhou, K. Zhou, S. Wang, F. Shen, Y. Gong, J. Gao, S. Liu, K. Guo, High-order acoustic vortex field generation based on a metasurface. *Phys. Rev. E* **100**, 053315 (2019).
24. H. L. Zhou, D. Z. Fu, J. J. Dong, P. Zhang, D. X. Chen, X. L. Cai, F. L. Li, X. L. Zhang, Orbital angular momentum complex spectrum analyzer for vortex light based on the rotational Doppler effect. *Light Sci. Appl.* **6**, e16251 (2017).
25. G. Li, T. Zentgraf, S. Zhang, Rotational Doppler effect in nonlinear optics. *Nat. Phys.* **12**, 736–740 (2016).
26. H. Zhou, D. Fu, J. Dong, P. Zhang, X. Zhang, Theoretical analysis and experimental verification on optical rotational Doppler effect. *Opt. Express* **24**, 10050–10056 (2016).
27. C. Zhang, L. Ma, Millimetre wave with rotational orbital angular momentum. *Sci. Rep.* **6**, 31921 (2016).
28. T. Yang, G. Wang, Rotational Doppler shift for electromagnetic waves carrying orbital angular momentum based on spectrum analysis. *AIP Conf. Proc.* **1820**, 090024 (2017).
29. M. P. J. Lavery, F. C. Speirits, S. M. Barnett, M. J. Padgett, Detection of a spinning object using light's orbital angular momentum. *Science* **341**, 537–540 (2013).
30. S. Qiu, T. Liu, Y. Ren, Z. Li, C. Wang, Q. Shao, Detection of spinning objects at oblique light incidence using the optical rotational Doppler effect. *Opt. Express* **27**, 24781–24792 (2019).
31. M. Zhao, X. Gao, M. Xie, W. Zhai, W. Xu, S. Huang, W. Gu, Measurement of the rotational Doppler frequency shift of a spinning object using a radio frequency orbital angular momentum beam. *Opt. Lett.* **41**, 2549–2552 (2016).
32. Y. Zhai, S. Fu, J. Zhang, Y. Lv, H. Zhou, C. Gao, Remote detection of a rotator based on rotational Doppler effect. *Appl. Phys. Exp.* **13**, 022012 (2020).
33. R. Wunenburger, J. I. V. Lozano, E. Brasselet, Acoustic orbital angular momentum transfer to matter by chiral scattering. *New J. Phys.* **17**, 103022 (2015).
34. S.-W. Fan, Y.-F. Wang, L. Cao, Y. Zhu, A. L. Chen, B. Vincent, B. Assouar, Y.-S. Wang, Acoustic vortices with high-order orbital angular momentum by a continuously tunable metasurface. *Appl. Phys. Lett.* **116**, 163504 (2020).
35. X. Jiang, Y. Li, B. Liang, J. C. Cheng, L. Zhang, Convert acoustic resonances to orbital angular momentum. *Phys. Rev. Lett.* **117**, 034301 (2016).
36. G. M. Gibson, E. Toninelli, S. A. R. Horsley, G. C. Spalding, E. Hendry, D. B. Phillips, M. J. Padgett, Reversal of orbital angular momentum arising from an extreme Doppler shift. *Proc. Natl. Acad. Sci. U.S.A.* **115**, 3800–3803 (2018).
37. M. Cromb, G. M. Gibson, E. Toninelli, M. J. Padgett, E. M. Wright, D. Faccio, Amplification of waves from a rotating body. *Nat. Phys.* **16**, 1069–1073 (2020).
38. B. Liu, S.-W. Wong, Y. Li, Rotational Doppler effect by space-time-coding metasurfaces for nonreciprocal electromagnetic isolation. *Opt. Express* **29**, 24500–24507 (2021).
39. M. A. B. Andrade, A. Marzo, J. C. Adamowski, Acoustic levitation in mid-air: Recent advances, challenges, and future perspectives. *Appl. Phys. Lett.* **116**, 250501 (2020).
40. A. A. Maznev, A. G. Every, O. B. Wright, Reciprocity in reflection and transmission: What is a 'phonon diode'? *Wave Motion* **50**, 776–784 (2013).
41. C. Shi, M. Dubois, Y. Wang, X. Zhang, High-speed acoustic communication by multiplexing orbital angular momentum. *Proc. Natl. Acad. Sci. U.S.A.* **114**, 7250–7253 (2017).
42. X. Jiang, B. Liang, J.-C. Cheng, C.-W. Qiu, Twisted acoustics: Metasurface-enabled multiplexing and demultiplexing. *Adv. Mater.* **30**, 1800257 (2018).
43. A. Marzo, B. W. Drinkwater, Holographic acoustic tweezers. *Proc. Natl. Acad. Sci. U.S.A.* **116**, 84–89 (2019).

Acknowledgments

Funding: This work was supported by the National Natural Science Foundation of China (61801183), the Natural Science Foundation of Guangdong Province (2019A1515011401 and 2018A0303130176), the Shanghai Science and Technology Committee (grant 21JC1405600), and the Guangdong Provincial Key Laboratory (2020B1212060066). **Author contributions:** Conceptualization: Q.W., M.G., and Y.L. Methodology: Q.W. and D.L. Experiments: Q.W., Z.Z., and H.D. Data analysis: Q.W., D.L., M.G., and Y.L. Supervision: M.G., Y.L., and D.L. Writing—original draft: Q.W., M.G., and Y.L. Writing—review and editing: Q.W., D.L., M.G., and Y.L. **Competing interests:** The authors declare that they have no competing interests. **Data and materials availability:** All data needed to evaluate the conclusions in the paper are present in the paper and/or the Supplementary Materials.

Submitted 8 April 2022
Accepted 22 August 2022
Published 5 October 2022
10.1126/sciadv.abq4451